Journal of Applied Sciences

ISSN 1812-5654

science alert

ANSInet
an open access publisher
http://ansinet.com

Journal of Applied Sciences 14 (10): 991-999, 2014
ISSN 1812-5654 / DOI: 10.3923/jas.2014.991.999

Modelling and Manoeuvrability Design of Autonomous Underwater Vehicle

Kiam Beng Yeo, Teck Ho Wong and Cheah Meng Ong
Unit Kajian Bahan dan Mineral, Sekolah Kejuruteraan dan Teknologi Maklumat,
Universiti Malaysia Sabah, Jalan UMS, 88400, Kota Kinabalu, Sabah, Malaysia

Abstract: This study presents a modelling and manoeuvrability design of a six Degree of Dreedom (DoF) hovering type Autonomous Underwater Vehicle (AUV) with emphasis on thrusters optimization and hydrodynamic effect. A six DoF kinematic and dynamic motion model has been developed and simulated in three-dimensional spaces for position tracking. The shape of the AUV and the location of thrusters are optimised considering the ability to provide the degree of freedom and stability of the system. The hydrodynamic effect of the AUV from the Computational Fluid Dynamic simulation was verified at 591 kPa of hydrostatic pressure on the surface for maximum depth up to 50 meters. Stalling phenomena was identified at 15° of pitching angle which caused unstable manoeuvring of the AUV. The study had also found that the hydrodynamic coefficients of lift and drag increases as the pitching angle increases with no significant effect due to Reynolds number changes (ReV = 9.53×10^4 to ReV = 2.86×10^5).

Key words: Autonomous underwater vehicle, flow trajectories, pitching angle, reynolds number

INTRODUCTION

Undersea exploration is demanding considering the vast, complex, unstructured and highly dynamic environment of the ocean. Despite of difficulties, the ocean attracts more and more attention from researchers due to the richness of ecology and geology system. As the quest to discover the ocean beyond human limits, underwater robotic system to replace humans has become more significant. In response, the Unmanned Underwater Vehicle (UUV) development thus gains momentum. Two distinct UUV type include the Remotely Operated Vehicle (ROV) and Autonomous Underwater Vehicle (AUV). An AUV is unmanned un-tethered underwater vehicle with on-board battery bank and relies on on-board circuits with pre-programmed artificial intelligence and commands to execute a mission. Whereas, ROV has the exact opposite characteristics compared to the AUV (Valavanis *et al*., 1997).

The earliest AUV application traced back to 1866, where an AUV carried explosive driven by compressed air was built by Robert Whitehead (Von Alt, 2003). Between the first AUV to 1990, there was limited AUV development and mostly unreported (Blidberg, 2001). In the 1990s, commercial application of AUV was finally possible due to healthy economic growth triggered by worldwide interest. As a result, about 30 AUVs were built worldwide within the decade. These activities contributed to advancement in materials, computation, sensory and as well as theoretical achievement in the field of AUV (Yuh, 2000).

AUVs were mainly divided into two types, based on its functionality and manoeuvring characteristic (Liu, 1992). A cruising type AUV being suitable for long range operation; used for systematic survey or search and for continuous operation. Whereas, hovering type AUV usually operates within a boundary; used in localize search and inspection and remain still during most tasks execution. Hovering type AUV requires three orthogonal movement and three moments in roll, pitch and yaw to overcome the stability in the dynamic environment; while cruising type AUV only requires three degrees of freedom movements which are longitudinal, yaw and pitch (Valavanis *et al*., 1997).

Modelling and manoeuvrability design of AUV requires a mathematical computation of rigid body kinematics involving Euler angles and six DoF kinematics. Several researchers (Yuh, 2000; Evans and Nahon, 2004; Kumar *et al*., 2005) had proposed different dynamic modelling for underwater robotic vehicles which utilizes the Newtonian and Lagrangian mechanics, hydrodynamic effects and characteristics, gravity, buoyancy and thruster dynamics. In addition, control techniques depending on linearization of motion about a single forward operating speed being not applicable to hovering AUV as it usually had comparable velocities along all

Corresponding Author: Kiam Beng Yeo, Unit Kajian Bahan dan Mineral, Sekolah Kejuruteraan dan Teknologi Maklumat, Universiti Malaysia Sabah, Jalan UMS, 88400, Kota Kinabalu, Sabah, Malaysia
Tel: +6088320000 Ext: 3236

three axes in the ocean compared to aircrafts and submarines (Antonelli, 2006). Various external forces and moments acting on and around the AUV and the added mass aspect of the dense ocean medium must also be considered. Therefore, the additional inertia terms to rigid body inertia terms must be introduced to account for the effective mass of surrounding fluid that must be accelerated with the vehicle (Yuh, 1990).

An essential quality for hovering AUV is their ability to manoeuvre accurately in the ocean. Until now, most of the literature had focused on designing control laws and little is known about thrust allocation (Yuh, 1994). In Whitcomb and Yoerger (1999), the research had been concentrated on finding the optimum thrusters configuration for underwater vehicle using one-norm algorithm to compare with modified singular values method. The relationship between the forces and moments and propeller thrust is a complicated function that depends on the vehicle's velocity, the water density, the tunnel length and cross-sectional area, the propeller's diameter and revolutions (Chin *et al*., 2006). A detailed analysis of the effect of thruster dynamics (Garus, 2004; Fossen, 1994), on the AUV thus becomes significant, especially in slow and fine motion (Inzartsev, 2009).

MATERIALS AND METHODS

Governing equation: The theoretical modelling of the AUV in 6-DOF is an important initiation to the introduction of kinematics. Then, formulation of Newtonian mechanics is implemented to derive the dynamics of the rigid body in translational and rotational motion.

Coordinate frame: The motion of the body-fixed frame is described relative to an inertial reference frame. For the AUV, it is assumed that the earth-fixed reference frame XYZ can be located at the inertial. This suggests that the position and orientation of AUV should be described to the inertial reference frame while linear and angular velocities of the vehicle should be expressed in the body-fixed coordinate system, as shown in Fig. 1.

Rigid body inertia matrix, M_{RB}: In order to obtain the rigid body inertia matrix, Euler's first and second axioms were applied to derive the rigid body equations of motion. Consider a body-fixed coordinate system X_o Y_o Z_o rotating with an angular velocity $\omega = [\omega 1, \omega 2, \omega 3]^T$ about an earth-fixed coordinate system X Y Z (Fig. 2). The M_{RB} referred to an arbitrary body-fixed coordinate system with origin O in the body-fixed frame is defined as:

$$M_{RB} = M_{RB}^{T} > 0;\ \dot{M}_{RB} = 0$$

$$M_{RB} = \begin{bmatrix} m & 0 & 0 & 0 & mz_G & my_G \\ 0 & m & 0 & -mz_G & 0 & mx_G \\ 0 & 0 & m & my_G & -mx_G & 0 \\ 0 & -mz_G & my_G & I_x & -I_{xy} & -I_{xz} \\ mz_G & 0 & -mx_G & -I_{yx} & I_y & -I_{yz} \\ -my_G & mx_G & 0 & -I_{zx} & -I_{zy} & I_z \end{bmatrix} \quad (1)$$

Coriolis and centripetal matrix, $C_{RB}(v)$: On the contrary, it is possible to find a large number of parameterizations for the $C_{RB}(v)$ matrix which consists of the Coriolis vector term and the centripetal vector term. Kirchhoff's

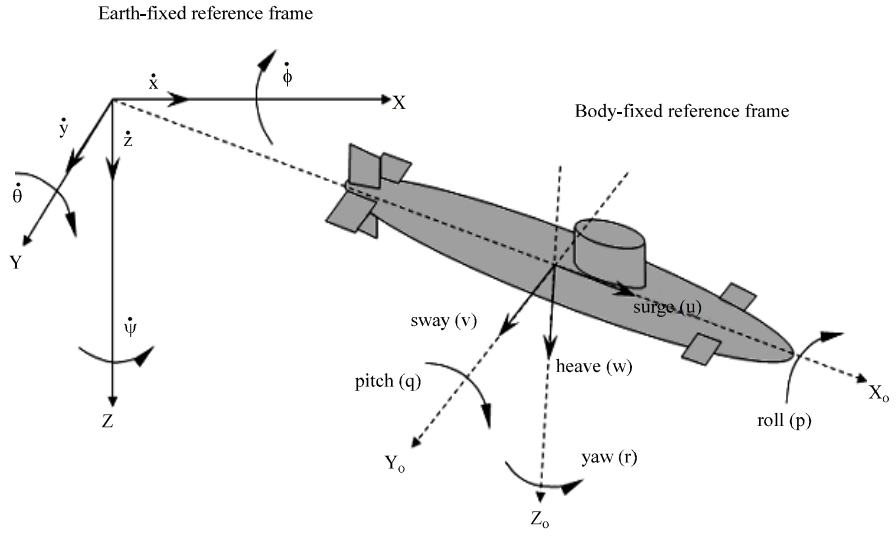

Fig. 1: Reference frames and dynamic variables of AUV

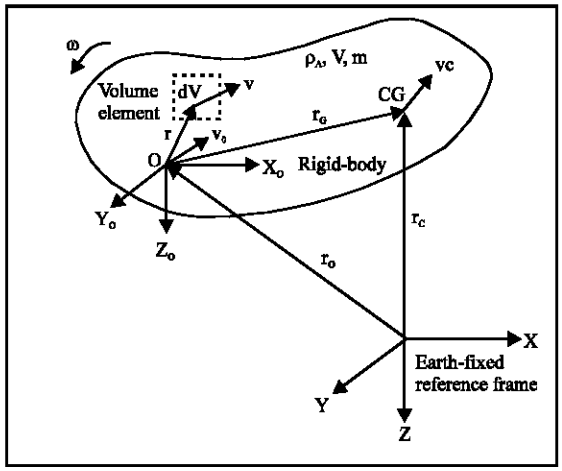

Fig. 2: The inertial, reference earth-fixed non-rotating frame XYZ and body-fixed rotating frame X_o Y_o Z_o

equations are implemented to derive a skew-symmetric representation of $C_{RB}(v)$. Therefore, the Coriolis and centripetal matrix, $C_{RB}(v)$ is defined in Eq. 2:

$$C_{RB}(v) = \begin{bmatrix} 0 & 0 & 0 & m(y_G q + z_G r) & -m(x_G q - w) & -m(x_G r + v) \\ 0 & 0 & 0 & -m(y_G p + w) & m(z_G r + x_G p) & -m(y_G r + u) \\ 0 & 0 & 0 & -m(z_G p - v) & -m(z_G p + u) & m(x_G p + y_G q) \\ -m(y_G q + z_G r) & m(y_G q + w) & m(z_G p - v) & 0 & -I_{yz} q - I_{xz} p + I_z r & I_{yz} r + I_{xy} p - I_x q \\ m(x_G q - w) & -m(z_G r + x_G p) & m(z_G p + u) & I_{yz} q + I_{xz} p - I_y r & 0 & I_{xz} q + I_{xy} p - I_x p \\ m(x_G q + v) & m(y_G r - u) & -m(x_G p + y_G q) & -I_{yz} r + I_{xz} p - I_x q & I_{xz} r + I_{xz} q - I_x p & 0 \end{bmatrix} \quad (2)$$

Total hydrodynamic damping matrix, D(v): In basic hydrodynamics, it is common to ensure that hydrodynamic forces and moments on a rigid body can be linearly superposed by considering two sub-problems that are Radiation-Induced Forces and Froude Froude-Kriloff and Diffraction Forces. Radiation-Induced Forces defined as forces on the body being forced to oscillate with the wave excitation frequency and there are no incident waves. Thus, it can be expressed mathematically as:

$$\tau R = -Dp(v)v - g(\eta) \quad (3)$$

In addition to radiation-induced potential damping, other damping effects like skin friction, wave drift damping and damping due to vortex shedding such that:

$$\tau D = -D_S(v)v - D_W(v)v - D_M(v)v \quad (4)$$

Implies the hydrodynamic forces and moments τ_H to be written as the sum of τ_R and τ_D, as:

$$\tau_H = \tau_R + \tau_D = -D(v)v - g(\eta) \quad (5)$$

where, the total hydrodynamic damping matrix D(v) is defined as:

Table 1: Comparison of various AUV shapes

Shapes	Advantages	Disadvantages
Single sphere	Low weight/vol. (W/V) ratio, excellent for deep diving vehicles	Low optimum vehicle length/diameter (L/D) ratio
Cylinder	Ease of fabrication, high optimum vehicle L/D ratio	High W/V ratio, end closures
Saucer	Improved hydrodynamics in horizontal plane, ease of hovering in currents	Inefficient structure, low controllability, limited to shallow depths
Oval	Good hydrodynamics, good W/V ratio	Difficult to design and fabricate

$$D(v) = D_F(v) + D_S(v) + D_W(v) + D_M(v) \quad (6)$$

Restoring forces and moments matrix, g(η): In the hydrodynamic terminology, the gravitational and buoyant forces are called restoring forces. The gravitational force, F_G will act through the centre of gravity, r_G of the vehicle. Similarly, the buoyant force, F_B will act through the centre of buoyancy, r_B. The Euler angle representation of the hydrostatic forces and moments matrix can be defined as:

$$M_{RB}v + C_{RB}(v)v + D(v)v + g(\eta) = \tau_E + \tau \quad (7)$$

MANOEUVRABILITY DESIGN

The main concerns in manoeuvrability design of AUV includes the drag minimization, optimized thruster location, stability and design layout of AUV components. The design aimed at developing and optimizing the AUV performance for effective manoeuvrability to a maximum depth of 50 m. As general design approach, propulsion, submerging and shape profile were identified as major spects. As well as hydrodynamic damping, pressure, buoyancy and stability must be taken into consideration.

Hydrodynamics: The first design process engages on the hydrodynamics which deals with the problem of drag minimization. In other words, it concerns with the minimization of D(v) term in the Eq. 7. To determine the hydrodynamic damping term, it is essential to determine the shape profile of the AUV. From this, estimation of drag coefficient can be extracted from available data for approximation. However, more reliable and accurate data of the damping term can be obtained from simulation results of CFD software or experimental verification.

Several feasible AUV shapes were studied for the best profile design selection. Table 1 summarizes the comparison of different AUV shapes. Spherical hulls offer the best structural integrity; however, the shape inhibits the efficient use of the space available as most components and systems are rectangular. Cylindrical hulls provide the better option, comprising high structural integrity and a shape conducive to the housing of electronic components. However, end closures caused

increase hydrodynamic drag and prohibited smooth controllability of the vehicle underwater in various DoF.

Saucer shape of hull limits the DoF of the AUV in roll, pitch and heave motion. Consequently, an oval shape hull was adopted in this specific design to take into account the operation requirements to achieve better manoeuvring control of the AUV.

Propulsion system: Propulsion is one of the most important systems on all AUVs and also a main sources of power consumption. The location of which motor affects the DoF can be controlled and positioned to reduce noise interference with onboard electronic components, as well as propeller-to-hull and propeller-to-propeller interactions. Propeller-to-hull and propeller-to-propeller interactions can have unwanted effects in the dynamics of an AUV.

Preferable both actuations of the AUV to be aligned with the drag force, at least for pure longitudinal, lateral and vertical motions for minimum drag force. This alignment ensures that, for constant velocities, the vehicle will not endure any moment on roll, pitch and yaw, thus, facilitating control design and improving control performance. For instance, to ensure symmetry, the horizontal motors are positioned laterally and vertically equidistant from the hulls; hence induce better stability and less problematic modelling of the vehicle. The symmetry also consequently aligns the centre of drag with the centre of thrust.

Submerging: The volume of the AUV remains constant, in order to dive, so it must increase the downward acting force acting to counteract the buoyant force. This can be accomplished by increasing its mass via the use of ballast tanks or by using of external thrusters. To reduce the size of ballast tanks or the force required by thrusters for the process of submerging, AUVs are usually designed so as to have residual buoyancy. That is, the weight of the vehicle is made to be more or less equal to the buoyant force.

The total expected mass of the vehicle also determine to a great extent the total AUV volume available. Large volume as opposed to mass would create too much buoyancy and thus, the vertical motors would require more thrust to keep the vehicle submerged. On the other hand, the volume was not large enough to counteract the mass, the vehicle would sink. For neutrally buoyant case, the buoyancy force F_B equals to the gravity force, F_G given by:

$$F_B = F_G \tag{8}$$

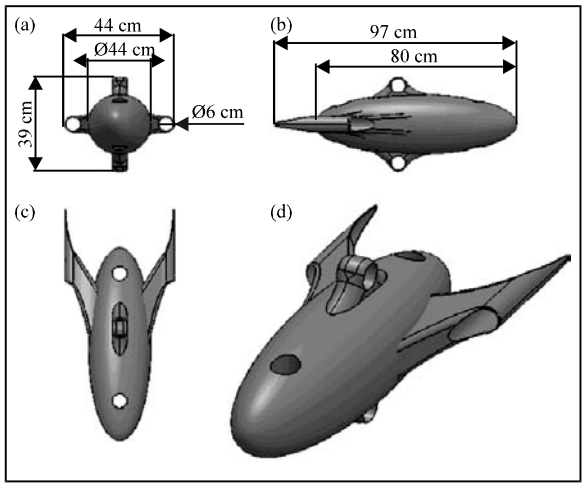

Fig. 3(a-d): Shape profile design of AUV. (a) Front view, (b) Side view, (c) Top view and (d) Trimetric view

$$\rho g V = mg \tag{9}$$

$$998.19\frac{kg}{m^3}\times 9.81 m sec^{-2}\times V m^3 = mkg\times 9.81 m sec^{-2}$$

$$V = (1.002\times 10^{-3}) m\ m^3 \tag{10}$$

Equation 10 suggests that for every 1 kg of mass, about 1.002×10^{-3} m^3 of volume should exist to ensure neutral buoyant condition.

Shape profile design: By the concepts discussed above, several designs were conceptualized for the AUV. The most feasible and physically realizable shape profile design is shown in Fig. 3. Smooth surface of the body hull ensures better hydrodynamics effect of the AUV and provides improved ability to withstand high pressure underwater. The top and bottom thrusters' mounting has also been designed for better structural performance. However, maintenance, inspection and addition of components would be inhibited due to limited space.

RESULTS AND DISCUSSION

The 3-D AUV design was subjected to computational analysis and simulation of flow trajectories constituting of velocity flow and pressure distribution on the AUV. Thus, the fluid interactions and manoeuvrability design of the AUV are correlated and discussed.

Simulation of flow trajectories: The CFD analysis conducted examines effects of external current

on the body of the AUV, ranging from 0.4 m sec^{-1} (Re_V = 9.53×10^4) to 1.2 m sec^{-1} (Re_V = 2.86×10^5) for different angles of attack (pitching angle). The range of current velocity was based on modelling of sea surface current circulation obtained from satellite altimetry data (Marghany and Hashim, 2005). The research was conducted to investigate typical water circulation characteristics during the inter-monsoon period of the South China Sea. It was realized that the maximum current flow magnitude was 1.2 m sec^{-1} and the minimum being 0.4 m sec^{-1}. Several other important parameters were also considered in the flow trajectories analysis for the CFD simulation. Table 2 listed the basic parameters that were defined in the process of the analysis. Some simulation results for current speed of 0.4 m sec^{-1} are shown in Fig. 4-6 for various pitching angles showing flow trajectories being stable and predominantly laminar.

Pressure distribution contour: The CFD analysis was also conducted to investigate the pressure distribution around the AUV at different pitching angle for various current velocities, ranging from 0.4-1.2 m sec^{-1}. Examples of several simulation results are shown in Fig. 7-9 where the pressure contour reference shown on the left of the figure depicts the total pressure exerted on the AUV which includes the hydrostatic pressure and the dynamic pressure terms.

Surging velocity and displacement of AUV: From the previous section, the 6-DOF rigid body equation of motion was derived and shown in Eq. 7. However, instead

Table 2: Parameters involved in simulation for 0.4 m sec^{-1} of current flow velocity

Parameter	Description
Thermodynamic	Static Pressure: 101325 Pa
	Temperature: 293.2 K
Velocity	Velocity vector
	Velocity in X direction: 0 m sec^{-1}
	Velocity in Y direction: 0 m sec^{-1}
	Velocity in Z direction: -0.4 m sec^{-1}
Turbulence	Turbulence intensity and length
	Intensity: 0.1 %
	Length: 0.003106 m
Wall condition	Adiabatic wall
Flow type	Laminar and turbulent
Fluid	Liquid-Water

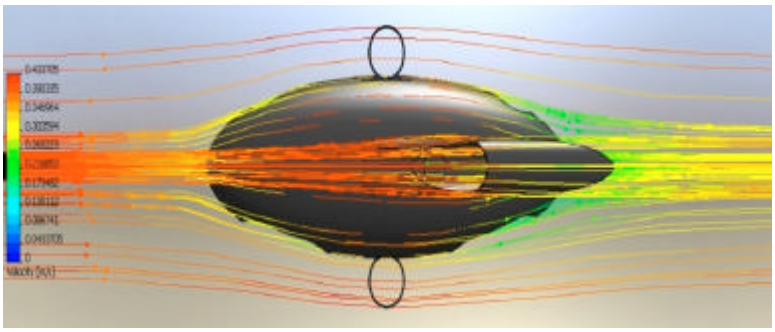

Fig. 4: Velocity flow trajectories for 0.4 m sec^{-1} of current speed at 0° pitching angle

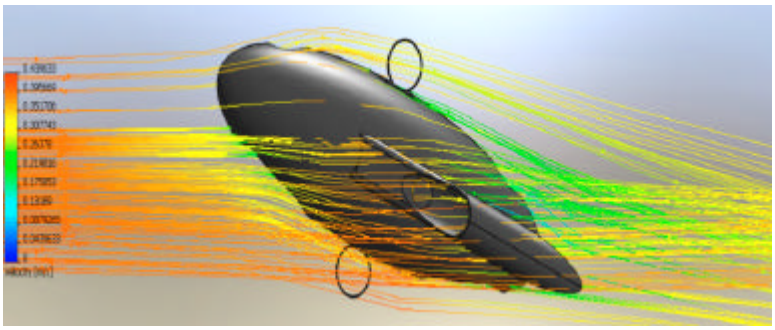

Fig. 5: Velocity flow trajectories for 0.4 m sec^{-1} of current speed at 20° pitching angle

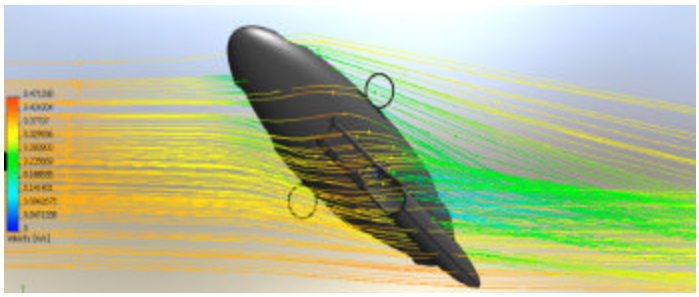

Fig. 6: Velocity flow trajectories for 0.4 m sec^{-1} of current speed at 40° pitching angle

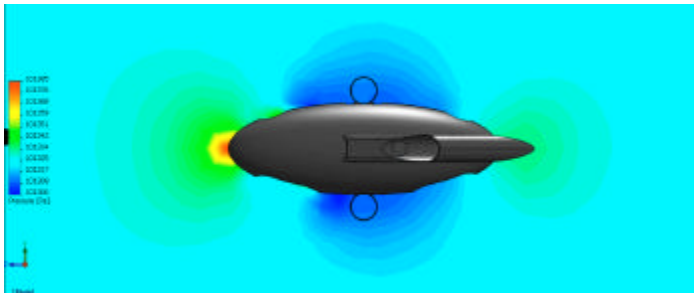

Fig. 7: Pressure distribution of AUV for 0.4 m sec^{-1} current speed at 0° pitching angle

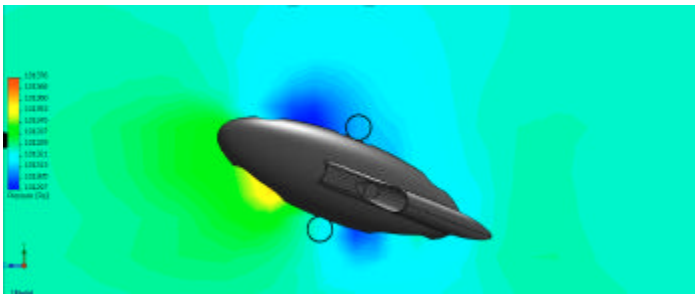

Fig. 8: Pressure distribution of AUV for 0.4 m sec^{-1} current speed at 20° pitching angle

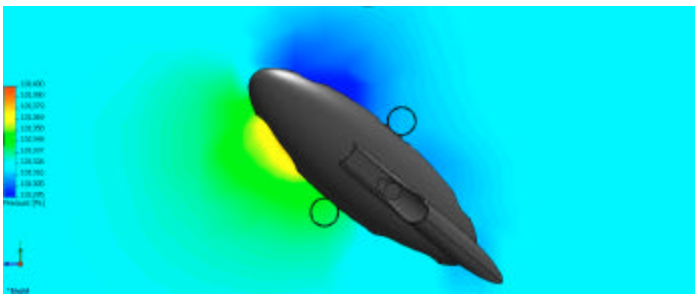

Fig. 9: Pressure distribution of AUV for 0.4 m sec^{-1} current speed at 40° pitching angle

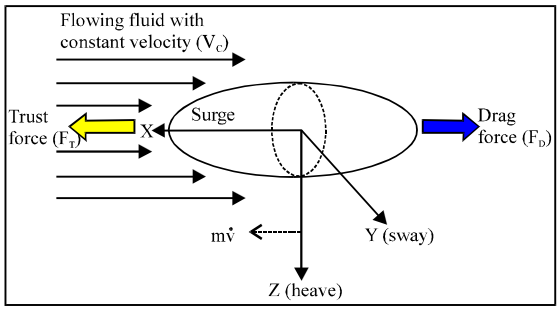

Fig. 10: Force analysis for translational motion of the AUV in 2-D plane

of solving Eq. 7 which incorporated all terms and being complex, the translational motion in 2-D plane was aslo considered (Fig. 10). In 2-D translation motion, the coriolis and centripetal term, $C_{RB}(v)$ and the restoring forces and moments term, $g(\eta)$ term, could be ignored. Besides that, by considering neutrally buoyant condition and total submerged environment, the radiation potential damping and wave drifting damping could also be neglacted. Thus, Eq. 7 could be simplied into:

$$M_{EB}v+D(v)v = \tau \quad (11)$$

The Eq. 11 was then solved to obtain the desired velocities and displacement of the AUV when deployed in flowing current velocities of 0.4 m sec^{-1}. Software solves the nonlinear secondary differential equation by implementing numerical method solution using explicit Runge-Kutta formulations. The results obtained are shown in Fig. 11.

From Fig. 11, it could be observed that thrust force, F_T of 1.5 N is required for the AUV to possess positive surging velocity of 0.18 m sec^{-1}. As the thrust force increases, the AUV will accelerate initially and surge with higher velocity after steady state condition has been achieved. Figure 11 also depicts the displacement undergone by the AUV in the first 10 sec of the travelling time with 0.4 m sec^{-1} of opposing current velocity. It has clearly shown that with no thrust force, the vehicle moves backward from the initial deployed position which is denoted by the negative displacement.

Stalling phenomena: The lift coefficient was computed for various pitching angles at the current velocity of 0.4 m sec^{-1} and the characteristic curve plotted as in Fig. 12. From the Figure, it shown that the lift coefficient, C_L increases in a nonlinear pattern as pitching angle, α increases. Further, the lift coefficient starts to drop tremendously at two regions which are approximately

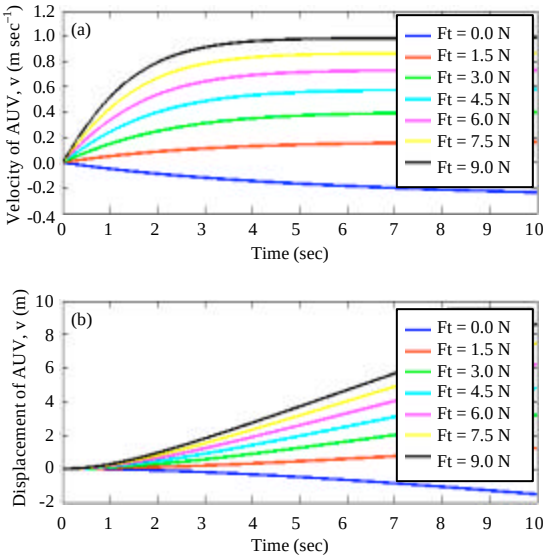

Fig. 11(a-b): Surging (a) Velocity, (b) Displacement of AUV vs time domain at 0.4 m sec^{-1} flow speed

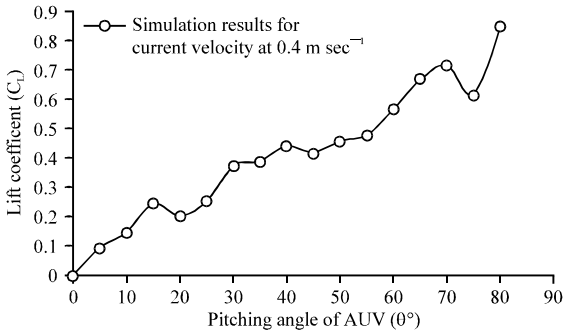

Fig. 12: Lift coefficient versus pitching angle of AUV

between the range of 15-20 degrees and 70-75 degrees. For effective manoeuvres and controllability of the AUV, it is crucial that the vehicle always operates in a stable climbing condition. Tremendous drop of the lift coefficient causes instability condition to the cruising of the vehicle. The sudden drop of lift force denotes impulsive lost on provision of the external lift force from the fluid flows and cause disturbances to trimmed cruising condition, hence, prohibit the AUV from manoeuvring to the desired pitching angle.

Lift coefficient and drag coefficient: The lift coefficient and drag coefficient with respect to current velocities ranging from 0.4-1.2 m sec^{-1}at various pitching angles are shown in Fig. 13 and 14, respectively. Figure 13 showed a massive increase in lift coefficient, C_L by 41, 156,

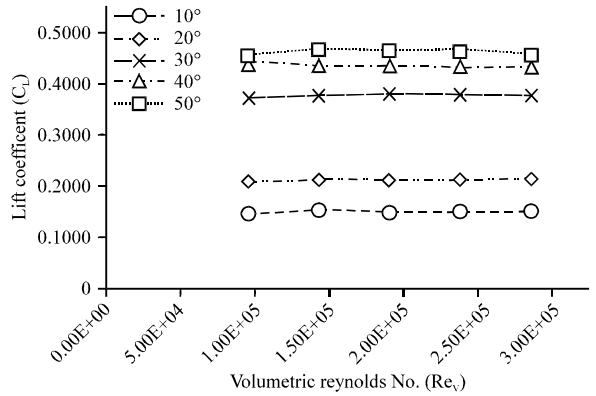

Fig. 13: Lift coefficient vs. volumetric Reynolds No. for $Re_V = 9.53\times10^4$ to $Re_V = 2.86\times10^5$ at various pitching angles

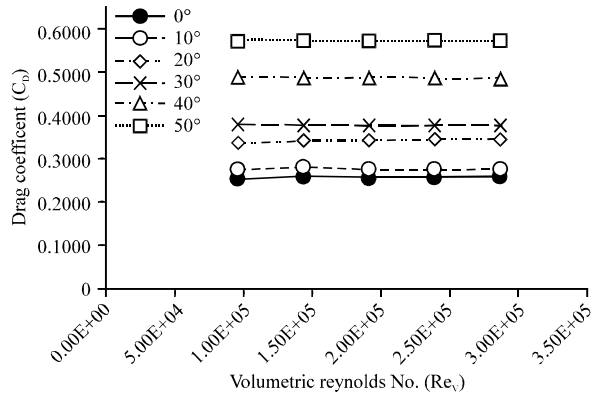

Fig. 14: Drag coefficient vs. volumetric Reynolds No. for $Re_V = 9.53\times10^4$ to $Re_V = 2.86\times10^5$ at various pitching angles

203 and 214% as pitching angle, θ increases from 10-20°, 30, 40 and 50° for $Re_V = 5.53\times10^4$. This could be attributed to the fact that increases of pressure force with increases in pitching angle resembling the blockage effect.

At higher pitching angles, the flow separation shifts from stern to the bow part of the body and it creates high pressure region over the bottom surface of the AUV. Hence, the uplift force acting on the body coupled with excess force generated due to high pressure region increases overall lift force acting on the body. It is also observed that as Re_V increased, lift coefficient remains constant with insignificant changes for all pitching angle. Figure 14 depicts the drag coefficient, D_D of the AUV produced by the current flow ranging from $Re_V = 9.53\times10^4$ to $Re_V = 2.86\times10^5$ at different pitching angle configurations. It is observed that drag coefficient increases by 7.82, 32, 48, 91 and 123% as pitching angle, θ increases from 0-10°, 20, 30, 40 and 50° for $Re_V = 9.53\times10^4$. The main cause of huge increase in C_D at pitching angles more than 20° has been due to the increase of normal pressure force exerted on the increasing frontal area as the AUV pitched for higher angles of elevation. It is further observed that as Re_V increases, C_D value remains constant with insignificant changes for all pitching angle. Reason for this behaviour of C_D may be atributed to the insignificant increase of flow velocity which remains as laminar, thus, provide comparable hydrodynamic effect with only very small changes of momentum impact on the AUV.

CONCLUSION

This study presented the modelling and manoeuvrability design of a 6-DoF hovering type AUV which contemplate on close structure shape selection, thruster's location optimisation and the study of environment effect on the lift force, drag force and stall effect. The manoeuvrability study was achieved through virtual environment, where simulation was conducted to aid the development of an equation that describe the AUV movement with respect to the thrusters output and the environment effect.

The modelling of the AUV being developed via Newtonian mechanics approach and the 6-DOF dynamic equations of motion were derived throughout the process. The governing equations mainly constitute terms of rigid body inertia matrix, hydrodynamic damping matrix, restoring forces and moments, environmental and propulsion forces and moments. Subsequently, a feasible 3-D model of the AUV was designed through iterative method with CAD verification. Fluid interactions and manoeuvrability design analysis were achieved through implementation of CFD software. Stalling phenomena had been identified at 15° of pitching angle where unstable manoeuvring of the vehicle will occur when the AUV tends to operate beyond the critical angle. The simulation results concluded also showed that the lift coefficient and drag coefficient increases as the pitching angle increases, but the considered range of Reynolds number ($Re_V = 9.53\times10^4$ to $Re_V = 2.86\times10^5$) had no significant effect on these hydrodynamic coefficients.

ACKNOWLEDGMENT

The authors would like to express their appreciation to the Unit Kajan Bahan dan Mineral (Materials and Minerals Research Unit), School of Engineering and Information Technology, Universiti Malaysia Sabah and the Ministry of Higher Education of Malaysia for their support.

REFERENCES

Antonelli, G., 2006. Underwater Robots: Motion and Force Control of Vehicle-Manipulator Systems. Vol. 2, Springer-Verlag, Berlin Heidelberg, Germany.

Blidberg, D.R., 2001. The development of Autonomous Underwater Vehicles (AUV): A brief summary. Proceedings of the International Conference on Robotics and Automation, May 21-26, 2001, Seoul, Korea.

Chin, C.S., M.W.S. Lau, E. Low and G.G.L. Seet, 2006. Design of thrusters configuration and thrust allocation control for a remotely operated vehicle. Proceedings of the IEEE Conference on Robotics, Automation and Mechatronics, June 1-3, 2006, Bangkok, Thailand, pp: 1-6.

Evans, J. and M. Nahon, 2004. Dynamics modeling and performance evaluation of an autonomous underwater vehicle. Ocean Eng., 31: 1835-1858.

Fossen, T.I., 1994. Guidance and Control of Ocean Vehicles. 1st Edn., Wiley, Chichester, UK., ISBN-13: 9780471941132, Pages: 494.

Garus, J., 2004. Optimization of thrust allocation in the propulsion system of an underwater vehicle. Int. J. Applied Math. Comput. Sci., 14: 461-467.

Inzartsev, A.V., 2009. Underwater Vehicles. In-Tech Publication, Zagreb, Croatia.

Kumar, R.P., A. Dasgupta and C.S. Kumar, 2005. Real-time optimal motion planning for autonomous underwater vehicles. Ocean Eng., 32: 1431-1447.

Liu, Y.K., 1992. AUVs' trends over the world in the future decade. Proceedings of the Symposium on Autonomous Underwater Vehicle Technology, June 2-3, 1992, Washington, DC., USA., pp: 116-127.

Marghany, M. and M. Hashim, 2005. Tsunami prediction along the malacca straits coastal waters. ASM-Asian GIS, remote sensing, positioning and surveying. South Pacific Science, December, 2005.

Valavanis, K. P., D. Gracanin, M. Matijasevic, R. Kolluru and G.A. Demetriou, 1997. Control architectures for autonomous underwater vehicles. IEEE Control Syst., 17: 48-64.

Von Alt, C.J., 2003. Autonomous underwater vehicles. Proceedings of the Autonomous Underwater Lagrangian Platforms and Sensors Workshop, March 31-April 1, 2003, La Jolla, CA., USA.

Whitcomb, L.L. and D.R. Yoerger, 1999. Development, comparison and preliminary experimental validation of nonlinear dynamic thruster models. IEEE J. Oceanic Eng., 24: 481-494.

Yuh, J., 1990. Modeling and control of underwater robotic vehicles. IEEE Trans. Syst. Man Cybernetics, 20: 1475-1483.

Yuh, J., 1994. Learning control for underwater robotic vehicles. IEEE Control Syst. Mag., 14: 39-46.

Yuh, J., 2000. Design and control of autonomous underwater robots: A survey. Autonom. Robots, 8: 7-24.